Preface

Fuel cell systems offer clean and efficient energy production and are currently under intensive development by several manufacturers for both stationary and mobile applications. The viability, efficiency, and robustness of the fuel cell technology depend on understanding, predicting, monitoring, and controlling the fuel cell system under a variety of environmental conditions and a wide operating range.

Many publications have discussed the importance and the need for a well-designed control system for fuel cell power plants. From discussions with control engineers and researchers in the area of fuel cell technology it became apparent that a comprehensive book with a control-oriented approach to modeling, analysis, and design was needed. The field is fast evolving and there is a lot of excitement but also a lot of commercial or confidentiality considerations that do not allow state-of-the-art results to be published.

In this book, we address this need by developing phenomenological models and applying model-based control techniques in polymer electrolyte membrane fuel cell systems. The book includes:

- An overview and comprehensive literature survey of polymer electrolyte membrane fuel cell systems, the underlying physical principles, the main control objectives, and the fundamental control difficulties.
- System-level dynamic models from physics-based component models using flow characteristics, point-mass inertia dynamics, lumped-volume manifold filling dynamics, time-evolving spatially homogeneous reactant pressure or concentration, and simple diffusion, transport, and heat equations.
- Formulation, in-depth analysis, and detailed control design for two critical control problems, namely, the control of the cathode oxygen supply for a high-pressure direct hydrogen Fuel Cell System (FCS) and control of the anode hydrogen supply from a natural gas Fuel Processor System (FPS).
- Multivariable controllers that address subsystem conflicts and constraints from sensor fidelity or actuator authority.

- Real-time observers for stack variables that may be hard to measure or augment existing stack sensors for redundancy in fault detection.
- Examples where control analysis not only can be used to develop robust controllers but also can help in making decisions on fuel cell system redesign for improved performance.
- More than 100 figures and illustrations.

This book is intended for researchers and students with basic control knowledge but who are novices in fuel cell technology. The simplicity of the models and the application of the control algorithms in concrete case studies should help practicing fuel cell engineers. Other scientists from electrochemistry, material sciences, and fluid dynamics who wish to become familiar with the control tools and methods may also benefit from the comprehensive coverage of the control design. Managers or entrepreneurs interested in accessing the challenges and opportunities in fuel cell automation technology may also find this book useful.

Book Overview

The development of a model of a dynamic fuel cell reactant supply subsystem that is suitable for control study is explained in Chapters 2 and 3. The model incorporates the transient behaviors that are important for integrated control design and analysis. Models of the auxiliary components, namely, a compressor, manifolds, an air cooler, and a humidifier, are presented in Chapter 2. Inertia dynamics along with nonlinear curve fitting of the compressor characteristic map are used to model the compressor. The manifold dynamic models are based on lumped-volume filling dynamics. Static models of the air cooler and air humidifier are developed using thermodynamics.

The fuel cell stack model in Chapter 3 is composed of four interacting submodels, namely, stack voltage, cathode flow, anode flow, and membrane hydration models. The stack voltage is calculated as a function of stack current, cell temperature, air pressure, oxygen and hydrogen partial pressures, and membrane humidity. The voltage function presented in Section 3.1 is based on the Nernst open circuit voltage, and activation, ohmic, and concentration losses. Flow equations, mass continuity, and electrochemical relations are used to create lumped-parameter dynamic models of the flow in the cathode and anode in Sections 3.2 and 3.3. Mass transport of water across the fuel cell membrane is calculated in the membrane hydration model in Section 3.4.

A perfect controller for air humidification and a simple proportional controller of the hydrogen supply valve are integrated into the model to allow us to focus on the analysis and control design of the air supply system. In Chapter 4, we perform a steady-state analysis of the model in order to determine the optimal value of the air flow setpoint, termed oxygen excess ratio, that results in the maximum system net power. The resulting value agrees

with the fuel cell specification in the literature, and thus indirectly validates the accuracy of the model. Results from the simulation of the model with a static feedforward controller based on the optimal setpoint are presented in Section 4.3. The model predicts transient behavior similar to that reported in the literature.

The control design of the air supply system using model-based linear control techniques is presented in Chapter 5. The goal of the control problem is to effectively regulate the oxygen concentration in the cathode by quickly and accurately replenishing oxygen depleted during power generation. Several control configurations are studied and the advantages and disadvantages of each configuration are also explained. Additionally, the performance limitations of the controller due to measurement constraints are also illustrated. In Section 5.5.2, the results from an observability analysis suggest the use of stack voltage measurement in the feedback to improve the performance of the observer-based controller. The analogy between the fuel cell closed-loop current-to-voltage transfer function and an electrical impedance, discussed in Section 5.6, can be useful to researchers in the area of power electronics. Section 5.7 presents an analysis of the tradeoff between regulation of cathode oxygen and desired net power during transient. A range of frequencies associated with the tradeoff is determined.

In Chapters 6 and 7, a control problem of the partial oxidation based natural gas fuel processor is studied. The components and processes associated with the processor are explained in Section 6.1. A dynamic model of the processor is also presented in Chapter 6. Transient flow, pressure, and reactor temperature characteristics are included. The reaction products are determined based on the chemical reactions, and the effects of both the oxygen-to-carbon ratio and the reactor temperature on the conversion are included. The model is validated with a high-order detailed model of the fuel cell and fuel processor system, and the results are shown in Section 6.3.

A two-input two-output control problem of regulating the catalytic partial oxidation (CPOX) temperature and the stack anode hydrogen concentration using natural gas valve and air blower commands is studied in Chapter 7. Section 7.3 illustrates the use of the relative gain array method to find appropriate pairings of the system input and output and also to analyze the system interactions. The analysis shows that large system interactions degrade the performance of the decentralized controller, especially during transient operation. A model-based multivariable controller for the fuel processor system is designed in Section 7.5 using the linear quadratic optimal method. It is shown that significant improvement in CPOX temperature regulation can be achieved with the designed multivariable controller. The controller is then analyzed to determine the important terms that contribute to the improvement of the closed loop performance. This will be useful in the simplification and implementation of the controller. Chapter 8 provides a summary and contributions of the work. Several topics that need to be addressed and several other interesting areas to study are also given.

The major technical topics covered in this book are:

- Two control problems of the fuel cell power generation system are formulated. The first problem is the control of the air supply system for a high-pressure direct hydrogen fuel cell system (FCS). The objective is to control the compressor motor command to quickly and efficiently replenish the cathode oxygen depleted during system power generations. The second problem is the control of a low-pressure natural gas fuel processor system (FPS). The goal is to coordinate an air blower and a fuel valve in order to quickly replenish the hydrogen depleted in the fuel cell anode while maintaining the desired temperature of the catalytic partial oxidation reactor.
- Control-oriented dynamic models suitable for control design and analysis are created. The complexity of the models is kept minimal by considering only physical effects relevant to the control problems. The models are developed using physics-based principles allowing them to be used for different fuel cell systems requiring only parameter modifications. Moreover, the variables in the models represent real physical variables providing insight into the dynamic behavior of the real system. The causality of the process is clearly demonstrated in the models.
- The models are used in the model-based control analysis to develop controllers and to determine required control structures that provide an enhanced performance over conventional controllers. Moreover, the analysis provides insight into the performance limitations associated with plant architecture, sensor location, and actuator bandwidth.
  - For the FCS, the limitations of using integral control and an observer-based controller arise from sensor locations. In particular, a direct measurement of the performance variable (*i.e.*, the oxygen excess ratio) is not possible. The compressor flow rate, which is located upstream from the stack, is traditionally used as the only feedback to the controller. Our observability analysis shows that the stack voltage measurement can be used to enhance the closed-loop system performance and robustness. The voltage measurement is currently used only for safety monitoring. However, we demonstrate that the fuel cell stack mean voltage can be used for active control of fuel cell stack starvation. This result exemplifies the power of control-theoretic tools in defining critical and cost-effective sensor location for the FCS.
  - An additional limitation arises when the FCS architecture dictates that all auxiliary equipment is powered directly from the fuel cell with no secondary power sources. This plant configuration is preferred due to its simplicity, compactness, and low cost. We used linear optimal control design to identify the frequencies at which there is severe tradeoff between the transient system net power performance and the stack starvation control. The result can be used to determine the required size of additional energy or oxygen storage devices in the case where fast transient response is required. We demonstrated that the multi-

variable controller improves the performance of the FCS and results in a different current–voltage dynamic relationship that is captured by the closed-loop FCS impedance. We expect that the derived closed-loop FCS impedance will be very useful and will provide the basis for a systematic design of fuel cell electronic components.

– Multivariable feedback analysis using the control-oriented model of the FPS indicates large system interactions between the fuel and the air loops at high frequencies. Our analysis shows that the magnitude and speed of the fuel valve limit the closed-loop bandwidth in the fuel loop, and thus affect hydrogen starvation. We demonstrate that fast regulation of CPOX temperature, which is the objective in the air loop, requires a fast blower and air dynamics if a decentralized control structure is used. On the other hand, a slow blower can also accomplish similar performance if it is coordinated with the fuel valve command. The coordination is achieved with a model-based controller that decouples the two loops at the frequencies of high interaction. With this result we provide rigorous guidelines regarding actuator specifications and the necessary software complexity for multiple actuator coordination.

Acknowledgments

We would like to the acknowledge the support of the Royal Thai government, the Automotive Research Center at the University of Michigan, and the National Science Foundation for their financial support during the period in which this manuscript was written.

We wish to thank Subbarao Varigonda, Jonas Eborn, Thordur Runolfsson, Christoph Haugstetter, Lars Pedersen, Shubhro Ghosh, Scott Bortoff, and Clas A. Jacobson from the United Technology Research Center for their help and for sharing with us their knowledge of fuel processor systems. We are grateful to Scott Staley, Doug Bell, Woong-Chul Yang, and James Adams of the Ford Motor Company for their encouragement and for providing valuable data on a vehicle fuel cell system.

At the University of Michigan, in the vehicle control laboratory and in the powertrain control laboratory we have worked alongside many talented students. Our thanks go to all of them. Thanks are also due to Dr. James Freudenberg and Dr. Erdogan Gulari from the University of Michigan for their help and advice.

Bangkok, Thailand — *Jay T. Pukrushpan*
Ann Arbor, Michigan — *Anna G. Stefanopoulou*
Ann Arbor, Michigan — *Huei Peng*
January 2004

2

Fuel Cell System Model: Auxiliary Components

Models developed specifically for control studies have certain characteristics. Important characteristics such as dynamic (transient) effects are included and some other effects, such as spatial variation of parameters, are neglected or approximated. Furthermore, only dynamic effects that are related to the automobile control problem are integrated into the models. The relevant time constants for an automotive propulsion-sized PEM fuel cell stack system are summarized in [56] as

- Electrochemistry O(10^{-19} sec),
- Hydrogen and air manifolds O(10^{-1} sec),
- Membrane water content O(unclear),
- Flow control/supercharging devices O(10^{0} sec),
- Vehicle inertia dynamics O(10^{1} sec), and
- Cell and stack temperature O(10^{2} sec),

where O denotes the order of magnitude. The fast transient phenomena of electrochemical reactions have minimal effects in automobile performance and can be ignored. The transient behaviors due to manifold filling dynamics, membrane water content, supercharging devices, and temperature may have an impact on the behavior of the vehicle and, thus, must be included in the model. The response of the humidification and membrane water content cannot be easily decoupled from the temperature and flow dynamics and, thus, the associated time constant is listed as "unclear". Interactions between processes, when appropriate, are also included. However, with relatively slow responses, the cell and stack temperature may be viewed as a separate control system which is equipped with a separate controller. The temperature can then be considered as a constant for other faster subsystems.

The system block diagram showing the subsystem blocks along with input/output signals is illustrated in Figure 2.1. The thick arrow between two component blocks (marked "flow") represents flow rate as well as the condition of the gas (*e.g.*, pressure, humidity, and temperature). In this and the next chapters, the models of several components shown in the figure are explained.

We focus on the reactant supply subsystem and thus the models of the components related to this subsystem are developed. The component models for the heat management subsystem are left for future study. Figure 2.2 illustrates the components and flows related to the reactant supply subsystem. It is assumed that the cathode and anode volumes of the multiple fuel cells are lumped as a single stack cathode and anode volumes. The anode supply and return manifold volumes are very small. Their sizes allow us to lump all these volumes to one "anode" volume. The cathode supply manifold lumps all the volumes associated with pipes and connections between the compressor and the stack cathode flow field. The length, and thus volume, of the cathode supply manifold can be large depending on the physical location of the compressor with respect to the stack. The cathode return manifold represents the lumped volume of pipes downstream from the stack cathode.

In this chapter, the modeling of the auxiliary components is explained. The compressor dynamic model is explained in Section 2.1 followed by an explanation of the manifold filling model in Section 2.2. Static models of the air cooler and the air humidifier are explained in Sections 2.4 and 2.5. In the next chapter, the development of the fuel cell stack model, which consists of stack voltage, anode flow, cathode flow, and membrane hydration models, is presented.

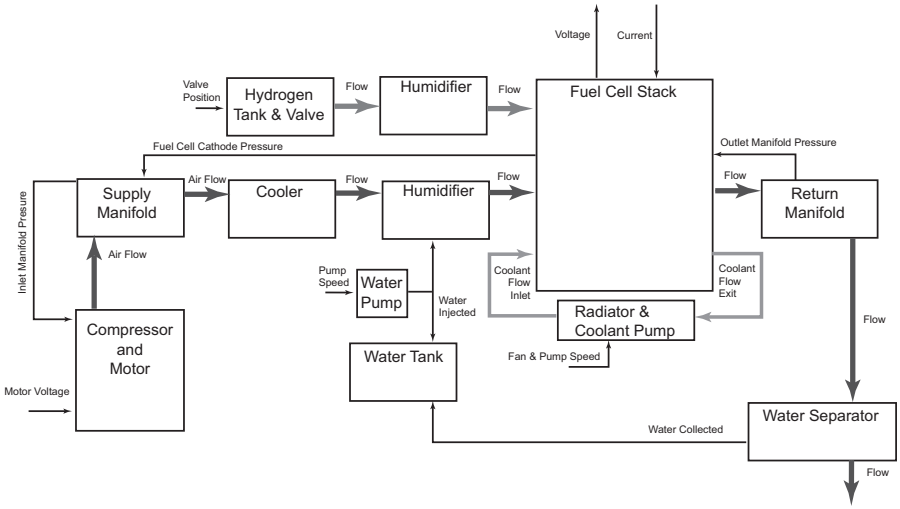

Fig. 2.1. System block diagram

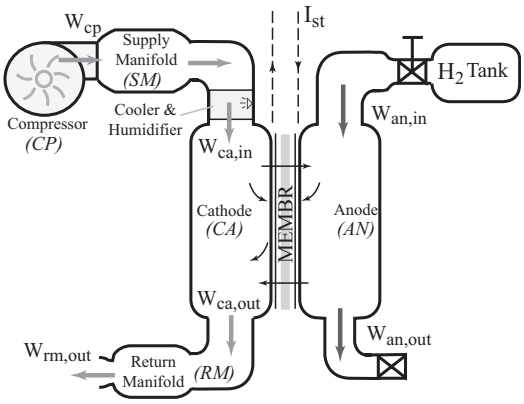

Fig. 2.2. Reactant supply subsystem model

2.1 Compressor Model

The compressor model is separated into two parts, as shown in Figure 2.3. The first part is a static compressor map which determines the air flow rate through the compressor. Thermodynamic equations are then used to calculate the exit air temperature and the required compressor power. The second part represents the compressor and motor inertia and defines the compressor speed. The speed is consequently used in the compressor map to find the air mass flow rate.

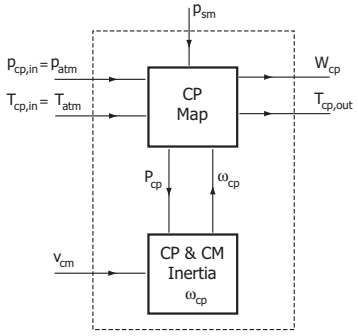

Fig. 2.3. Compressor block diagram

The only dynamic state in the model is the compressor speed ω_{cp}. The inputs to the model include inlet air pressure $p_{cp,in}$, its temperature $T_{cp,in}$, the voltage command to the compressor motor v_{cm}, and downstream pressure, which is the supply manifold pressure $p_{cp,out} = p_{sm}$. The inlet air is typically atmospheric and its pressure and temperature are assumed to be fixed at

$p_{atm} = 1$ atm and $T_{atm} = 25°$C, respectively. The motor command is one of the inputs to the fuel cell system. The downstream pressure is determined by the supply manifold model.

The compressor air mass flow rate W_{cp} (kg/sec) is determined, through a compressor flow map, from the pressure ratio across the compressor and the speed of the compressor. However, supplying the compressor flow map in the form of a look-up table is not well suited for dynamic system simulations [80]. Standard interpolation routines are not continuously differentiable and extrapolation is unreliable. Therefore, a nonlinear curve fitting method is used to model the compressor characteristics. The Jensen & Kristensen method, described in [80], is used in our model.

To reflect variations in the inlet condition of the compressor, which are the inlet flow pressure and temperature, the "corrected" values of mass flow rate and compressor speed are used in the compressor map. The corrected values [29] are the corrected compressor speed (rpm) $N_{cr} = N_{cp}/\sqrt{\theta}$, and the corrected mass flow $W_{cr} = W_{cp}\sqrt{\theta}/\delta$, where corrected temperature $\theta = T_{cp,in}/\ 288\ \mathrm{K}$ and corrected pressure $\delta = p_{cp,in}/\ 1\ $ atm. Using the Jensen & Kristensen method, the dimensionless head parameter Ψ is first defined:

$$\Psi = C_p T_{cp,in} \left[\left(\frac{p_{cp,out}}{p_{cp,in}} \right)^{\frac{\gamma-1}{\gamma}} - 1 \right] / \left(\frac{U_c^2}{2} \right) \tag{2.1}$$

where the inlet air temperature $T_{cp,in}$ is in Kelvin and U_c is the compressor blade tip speed (m/s),

$$U_c = \frac{\pi}{60} d_c N_{cr} \tag{2.2}$$

d_c is the compressor diameter (m), and γ is the ratio of the specific heats of the gas at constant pressure C_p/C_v, which is equal to 1.4 in the case of air. The normalized compressor flow rate Φ is defined by

$$\Phi = \frac{W_{cr}}{\rho_a \frac{\pi}{4} d_c^2 U_c} \tag{2.3}$$

where ρ_a is the air density (kg/m^3). The normalized compressor flow rate Φ is then correlated with the head parameter Ψ by the equation

$$\Phi = \Phi_{max} \left[1 - \exp\left(\beta \left(\frac{\Psi}{\Psi_{max}} - 1 \right) \right) \right] \tag{2.4}$$

where Φ_{max}, β, and Ψ_{max} are polynomial functions of the Mach number M,

$$\begin{aligned} \Phi_{max} &= a_4 M^4 + a_3 M^3 + a_2 M^2 + a_1 M + a_0 \\ \beta &= b_2 M^2 + b_1 M + b_0 \\ \Psi_{max} &= c_5 M^5 + c_4 M^4 + c_3 M^3 + c_2 M^2 + c_1 M + c_0 \end{aligned} \tag{2.5}$$

The inlet Mach number M is defined by

Table 2.1. Compressor map parameters

Parameter	Value	Units
R_a	2.869×10^2	J/(kg·K)
ρ_a	1.23	kg/m^3
d_c	0.2286	m

$$M = \frac{U_c}{\sqrt{\gamma R_a T_{cp,in}}} \tag{2.6}$$

where R_a is the air gas constant. In Equation (2.5), a_i, b_i, and c_i are regression coefficients obtained by curve fitting of the compressor data. The air mass flow in kg/sec is then calculated using Equation (2.3):

$$W_{cr} = \Phi \rho_a \frac{\pi}{4} d_c^2 U_c \tag{2.7}$$

The parameters used in the model are given in Table 2.1. The compressor model used here is for an Allied Signal compressor. The data were obtained by digitizing the compressor map given in [29]. The regression coefficients obtained by curve fitting are given in Table 2.2. Figure 2.4 shows that the curve fitting scheme represents the compressor data very well.

Table 2.2. Compressor map regression coefficients

Parameter	Value
a_4	-3.69906×10^{-5}
a_3	2.70399×10^{-4}
a_2	-5.36235×10^{-4}
a_1	-4.63685×10^{-5}
a_0	2.21195×10^{-3}
b_2	1.76567
b_1	-1.34837
b_0	2.44419
c_5	-9.78755×10^{-3}
c_4	0.10581
c_3	-0.42937
c_2	0.80121
c_1	-0.68344
c_0	0.43331

A look-up table of the compressor efficiency η_{cp} is used to find the efficiency of the compressor from the mass flow rate and pressure ratio across the compressor. The maximum efficiency of the compressor is 80%. The temperature of the air leaving the compressor is calculated from the equation

$$T_{cp,out} = T_{cp,in} + \frac{T_{cp,in}}{\eta_{cp}} \left[\left(\frac{p_{cp,out}}{p_{cp,in}} \right)^{\frac{\gamma-1}{\gamma}} - 1 \right]$$

$$= T_{atm} + \frac{T_{atm}}{\eta_{cp}} \left[\left(\frac{p_{sm}}{p_{atm}} \right)^{\frac{\gamma-1}{\gamma}} - 1 \right] \tag{2.8}$$

The torque required to drive the compressor is calculated using thermodynamic equation:

$$\tau_{cp} = \frac{C_p}{\omega_{cp}} \frac{T_{atm}}{\eta_{cp}} \left[\left(\frac{p_{sm}}{p_{atm}} \right)^{\frac{\gamma-1}{\gamma}} - 1 \right] W_{cp} \tag{2.9}$$

where τ_{cp} is the torque needed to drive the compressor in N-m;
C_p is the specific heat capacity of air $= 1004 \quad \mathrm{J \cdot kg^{-1} \cdot K^{-1}}$;
γ is the ratio of the specific heats of air $= 1.4$.

Derivations of Equations (2.8) and (2.9) are standard and can be found in the thermodynamics or turbine literature [21, 53].

A lumped rotational parameter model with inertia is used to represent the dynamic behavior of the compressor speed:

$$J_{cp} \frac{d\omega_{cp}}{dt} = (\tau_{cm} - \tau_{cp}) \tag{2.10}$$

where J_{cp} is the combined inertia of the compressor and the motor (kg·m^2);
ω_{cp} is the compressor speed (rad/sec);
τ_{cm} is the compressor motor torque input (N-m);
τ_{cp} is the torque required to drive the compressor (N-m).

The compressor motor torque is calculated using a static motor equation:

$$\tau_{cm} = \eta_{cm} \frac{k_t}{R_{cm}} (v_{cm} - k_v \omega_{cp}) \tag{2.11}$$

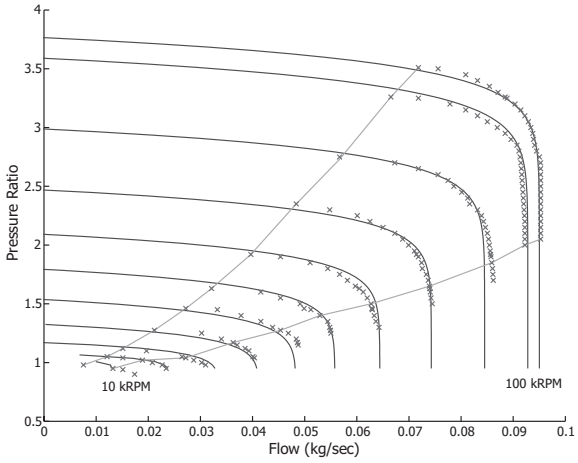

Fig. 2.4. Compressor map

where k_t, R_{cm}, and k_v are motor constants and η_{cm} is the motor mechanical efficiency. The values are given in Table 2.3.

Table 2.3. Compressor motor parameters

Parameter	Value
k_v	0.0153 V/(rad/sec)
k_t	0.0153 N-m/Amp
R_{cm}	0.82 Ω
η_{cm}	98%

2.2 Lumped Model of the Manifold Dynamics

The manifold model represents the lumped volume associated with pipes and connections between each device. The supply manifold volume includes the volume of the pipes between the compressor and the fuel cell stack including the volume of the cooler and the humidifier (Figure 1.5). The return manifold represents the pipeline at the fuel cell stack exhaust.

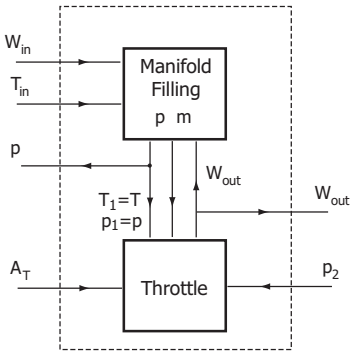

Fig. 2.5. Manifold block diagram

A block diagram of the manifold model is shown in Figure 2.5. The mass conservation principle is used to develop the manifold model. For any manifold,

$$\frac{dm}{dt} = W_{in} - W_{out} \tag{2.12}$$

where m is the mass of the gas accumulated in the manifold volume and W_{in} and W_{out} are mass flow rates into and out of the manifold. If we assume that the air temperature is constant in the manifold T and equal to the inlet

flow temperature $T = T_{in}$, the manifold filling dynamics follow an isothermic relation:

$$\frac{dp}{dt} = \frac{R_a T}{V}(W_{in} - W_{out}) \tag{2.13}$$

where R_a is the gas constant of air and V is the manifold volume. If the air temperature is expected to change in the manifold, the pressure dynamic equation, which is derived from the energy conservation, the ideal gas law, and the air thermodynamic properties,

$$\frac{dp}{dt} = \frac{\gamma R_a}{V}\left(W_{in}T_{in} - W_{out}T\right) \tag{2.14}$$

is used in addition to the mass balance equation (2.12). The air temperature T in (2.14) is calculated from the air mass m in (2.12) and air pressure p in (2.14) using the ideal gas law. In summary, if the temperature of the air in the manifold is assumed constant, Equation (2.13) is used to model the manifold dynamics. If the temperature of the air is expected to change, Equations (2.12) and (2.14) are used.

The nozzle flow equation, derived in [58], is used to calculate the outlet flow of the manifold. The flow rate passing through a nozzle is a function of the upstream pressure p_1, the upstream temperature T_1, and the downstream pressure p_2, of the nozzle. The flow characteristic is divided into two regions by the critical pressure ratio:

$$\left(\frac{p_2}{p_1}\right)_{crit} = \left(\frac{2}{\gamma+1}\right)^{\frac{\gamma}{\gamma-1}} \tag{2.15}$$

where γ is the ratio of the specific heat capacities of the gas C_p/C_v. In the case of air $\gamma = 1.4$ and the critical pressure ratio is equal to 0.528. For sub-critical flow where the pressure drop is less than the critical pressure ratio

$$\frac{p_2}{p_1} > \left(\frac{2}{\gamma+1}\right)^{\frac{\gamma}{\gamma-1}}$$

the mass flow rate is calculated from

$$W = \frac{C_D A_T p_1}{\sqrt{\bar{R}T_1}}\left(\frac{p_2}{p_1}\right)^{\frac{1}{\gamma}}\left\{\frac{2\gamma}{\gamma-1}\left[1-\left(\frac{p_2}{p_1}\right)^{\frac{\gamma-1}{\gamma}}\right]\right\}^{\frac{1}{2}} \quad \text{for } \frac{p_2}{p_1} > \left(\frac{2}{\gamma+1}\right)^{\frac{\gamma}{\gamma-1}} \tag{2.16}$$

For critical flow (or choked flow), the mass flow rate is given by

$$W_{choked} = \frac{C_D A_T p_1}{\sqrt{\bar{R}T_1}}\gamma^{\frac{1}{2}}\left(\frac{2}{\gamma+1}\right)^{\frac{\gamma+1}{2(\gamma-1)}} \qquad \text{for} \quad \frac{p_2}{p_1} \leq \left(\frac{2}{\gamma+1}\right)^{\frac{\gamma}{\gamma-1}} \tag{2.17}$$

Parameter C_D is the discharge coefficient of the nozzle, A_T is the opening area of the nozzle (m^2), and $\bar{R}$ is the universal gas constant. The plot of

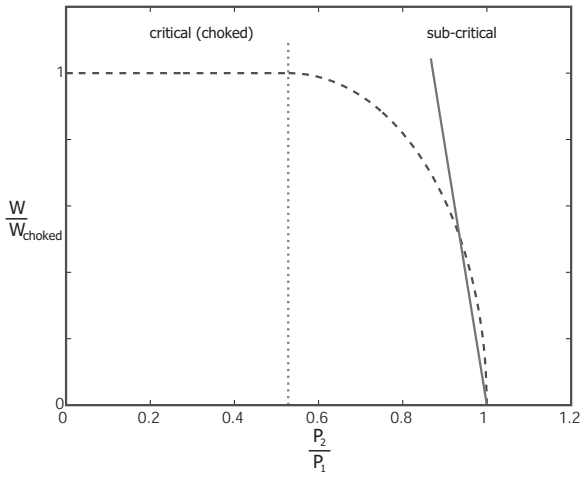

Fig. 2.6. Dashed line: relative mass flow rate as a function of nozzle pressure ratio (2.16)-(2.17); solid line: linearized mass flow rate at low pressure difference (2.18)

W/W_{choked} is shown as a dashed line in Figure 2.6. If the pressure difference between the manifold and the downstream volume is small and always falls into the subcritical flow region, the flow rate can be calculated by a linearized form of the subcritical nozzle flow equation (2.16),

$$W = k(p_1 - p_2) \tag{2.18}$$

where k is the nozzle constant. The plot of the linearized equation (2.18) for various manifold pressures is shown in Figure 2.7 as a solid line, compared to the plot of Equation (2.16) shown as a dashed line.

2.2.1 Supply Manifold

For the supply manifold, the inlet mass flow is the compressor flow W_{cp} and the outlet mass flow is $W_{sm,out}$. Because the pressure difference between the supply manifold and the cathode is relatively small,

$$W_{sm,out} = k_{sm,out}(p_{sm} - p_{ca}) \tag{2.19}$$

where $k_{sm,out}$ is the supply manifold outlet flow constant. Because the temperature of the air leaving the compressor is high, it is expected that the air temperature changes inside the supply manifold. Thus, Equations (2.12) and (2.14) are used to model the supply manifold

$$\frac{dm_{sm}}{dt} = W_{cp} - W_{sm,out} \tag{2.20}$$

$$\frac{dp_{sm}}{dt} = \frac{\gamma R_a}{V_{sm}} \left(W_{cp} T_{cp,out} - W_{sm,out} T_{sm}\right) \tag{2.21}$$

where V_{sm} is the supply manifold volume and T_{sm} is the supply manifold air temperature, which is calculated from m_{sm} and p_{sm} using the ideal gas law. A block diagram of the supply manifold is shown in Figure 2.8.

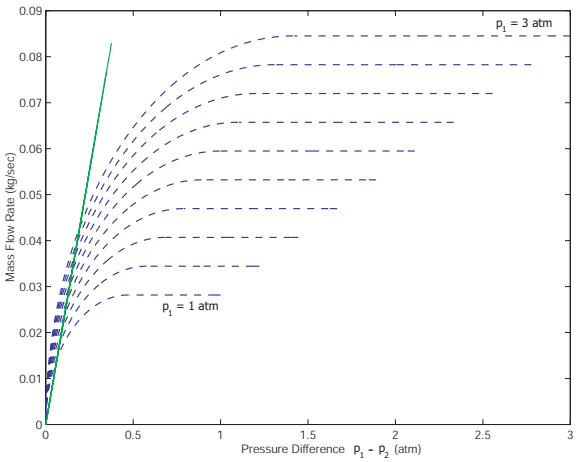

Fig. 2.7. Comparison of nozzle flow rate from nonlinear and linear nozzle equations

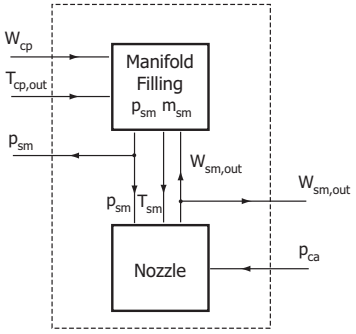

Fig. 2.8. Supply manifold block diagram

2.2.2 Return Manifold

The temperature of the air leaving the stack is relatively low. Therefore, the changes of air temperature in the return manifold are negligible, and the return manifold pressure is modeled by

$$\frac{dp_{rm}}{dt} = \frac{R_a T_{rm}}{V_{rm}}(W_{ca,out} - W_{rm,out}) \tag{2.22}$$

where V_{rm} is the return manifold volume and T_{rm} is the temperature of the gas in the return manifold. The flow entering the return manifold $W_{ca,out}$ is calculated in Equation (3.47), which is in the same form as Equation (2.19). The outlet mass flow of the return manifold is governed by nozzle (throttle) equations (2.16) to (2.17). The outlet mass flow is a function of the manifold pressure p_{rm} and the pressure downstream from the manifold, which is assumed to be fixed at p_{atm}. Because the pressure drop between the return manifold and the atmospheric is relatively large, the equations of the return manifold exit flow are

$$W_{rm,out} = \frac{C_{D,rm} A_{T,rm} p_{rm}}{\sqrt{\bar{R} T_{rm}}} \left(\frac{p_{atm}}{p_{rm}}\right)^{\frac{1}{\gamma}} \left\{ \frac{2\gamma}{\gamma - 1} \left[1 - \left(\frac{p_{atm}}{p_{rm}}\right)^{\frac{\gamma-1}{\gamma}} \right] \right\}^{\frac{1}{2}} \quad \text{for} \quad \frac{p_{atm}}{p_{rm}} > \left(\frac{2}{\gamma+1}\right)^{\frac{\gamma}{\gamma-1}} \tag{2.23}$$

and

$$W_{rm,out} = \frac{C_{D,rm} A_{T,rm} p_{rm}}{\sqrt{\bar{R} T_{rm}}} \gamma^{\frac{1}{2}} \left(\frac{2}{\gamma+1}\right)^{\frac{\gamma+1}{2(\gamma-1)}} \quad \text{for} \quad \frac{p_{atm}}{p_{rm}} \leq \left(\frac{2}{\gamma+1}\right)^{\frac{\gamma}{\gamma-1}} \tag{2.24}$$

The throttle opening area $A_{T,rm}$ can be set constant or can be used as an extra control variable to regulate the return manifold pressure, and thus the cathode pressure [97]. The values of $C_{D,rm}$ and the nominal value of $A_{T,rm}$ used in the model are given in Table 4.1. A block diagram of the return manifold model is shown in Figure 2.9.

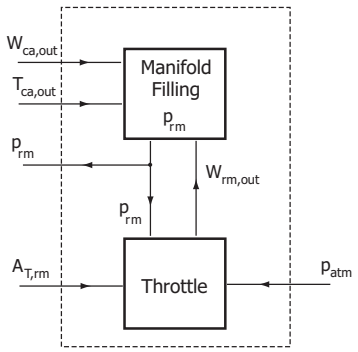

Fig. 2.9. Return manifold block diagram

The pressure calculated in the supply manifold model is used in the compressor model to determine the pressure ratio across the compressor. The

return manifold pressure calculated in the return manifold model is used to determine the flow rate exiting the fuel cell cathode. The model of the cathode along with other parts of the fuel cell stack are described in the next chapter.

2.3 Review of the Thermodynamics of Gas Mixtures

In this section, we review the basic thermodynamic properties of gas mixtures that we use extensively in the model. Details can be found in [103]. We also focus on the mixture involving gases and water vapor.

Here, we consider properties of ideal gases. Specifically, each component of the mixture is independent of the presence of other components and each component can be treated as an ideal gas. Consider the mixture of gas A and gas B. From the ideal gas law, we have

$$pV = n\bar{R}T = mRT \tag{2.25}$$

where p is the gas pressure, V is the gas volume, n is the number of moles of the gas, m is the mass of the gas, $\bar{R}$ is the universal gas constant, R is the gas constant, and T is the gas temperature. The total number of moles of the mixture is equal to the sum of the number of moles of each component:

$$n = n_A + n_B \tag{2.26}$$

If we treat each component as an ideal gas, the law in (2.25) holds for each component:

$$\begin{aligned} p_A V &= n_A \bar{R}T \\ p_B V &= n_B \bar{R}T \end{aligned} \tag{2.27}$$

where p_A and p_B are the partial pressures. By substitution of Equations (2.25) and (2.27) into Equation (2.26), we get

$$p = p_A + p_B \tag{2.28}$$

Thus, for a mixture of ideal gases, the pressure of the mixture is the sum of the partial pressures of the individual components.

Let us now consider a mixture of air and water vapor. The humidity ratio ω is defined as the ratio of the mass of water vapor m_v to the mass of dry air m_a:

$$\omega = \frac{m_v}{m_a} \tag{2.29}$$

The total mass of the mixture is $m_a + m_v$. The humidity ratio does not give a good representation of the humidity of the mixture because the maximum amount of water vapor that the air can hold (saturation) depends on the temperature and pressure of the air. The relative humidity, which represents the amount of water in the air relative to the maximum possible amount, is therefore more widely used. The relative humidity ϕ is defined as the ratio

of the mole fraction of the water vapor in the mixture to the mole fraction of vapor in a saturated mixture at the same temperature and pressure. With the assumption of ideal gases, the definition reduces to the ratio of the partial pressure of the water vapor p_v in the mixture to the saturation pressure of the vapor at the temperature of the mixture p_{sat}:

$$\phi = \frac{p_v}{p_{sat}} \tag{2.30}$$

The saturation pressure p_{sat} depends on the temperature and is easily obtained from a thermodynamic table of vapor [103]. In the model, the saturation pressure is calculated from an equation of the form given in [83]. The saturation pressure data in [103] is used to obtain the coefficients in the equation:

$$\begin{aligned}\log_{10}(P_{sat}) = -1.69 \times 10^{-10}T^4 + 3.85 \times 10^{-7}T^3 - 3.39 \times 10^{-4}T^2 \\ + 0.143\ T - 20.92\end{aligned} \tag{2.31}$$

where the saturation pressure p_{sat} is in kPa and the temperature T is in Kelvin.

The relation between the humidity ratio and the relative humidity can be derived from the ideal gas law:

$$\omega = \frac{m_v}{m_a} = \frac{p_v V/R_v T}{p_a V/R_a T} = \frac{R_a p_v}{R_v p_a} = \frac{M_v}{M_a}\frac{p_v}{p_a} \tag{2.32}$$

where M_v and M_a, both in kg/mol, are the molar mass of vapor and dry air, respectively. By using Equations (2.28) and (2.30), the relative humidity can be calculated from dry air pressure and the humidity ratio

$$\phi = \omega \frac{M_a}{M_v}\frac{p_a}{p_{sat}} \tag{2.33}$$

There are some details that should be pointed out. First, relative humidity having a value of one means that the mixture is saturated or fully humidified. If there is more water content in the mixture, the extra amount of water will condense into a liquid form. Second, with the ideal gas assumption, various components in the mixture can be treated separately when performing the internal energy and enthalpy calculations.

2.4 Air Cooler (Static) Model

The temperature of the air in the supply manifold is typically high due to the high temperature of air leaving the compressor. To prevent any damage to the fuel cell membrane, the air needs to be cooled down to the stack operating temperature. In this study, we do not address heat transfer effects and thus we

assume that an ideal air cooler maintains the temperature of the air entering the stack at $T_{cl} = 80°\text{C}$. It is assumed that there is no pressure drop across the cooler, $p_{cl} = p_{sm}$. Because temperature change affects gas humidity, the humidity of the gas exiting the cooler is calculated as

$$\phi_{cl} = \frac{p_{v,cl}}{p_{sat}(T_{cl})} = \frac{p_{cl}p_{v,atm}}{p_{atm}p_{sat}(T_{cl})} = \frac{p_{cl}\phi_{atm}p_{sat}(T_{atm})}{p_{atm}p_{sat}(T_{cl})} \tag{2.34}$$

where $\phi_{atm} = 0.5$ is the nominal ambient air relative humidity and $p_{sat}(T_i)$ is the vapor saturation pressure that is a function of temperature T_i. The change in temperature does not affect the mass of the gas; thus, the mass flow rate does not change in the cooler model; that is, $W_{cl} = W_{sm,out}$.

2.5 Humidifier (Static) Model

Air flow from the cooler is humidified before entering the stack by injecting water into the air stream in the humidifier. Here, the volume of the humidifier is small and hence it can be considered as part of the supply manifold volume. A static model of the humidifier is used to calculate the change in air humidity due to the additional injected water. The temperature of the flow is assumed to be constant; thus, $T_{hm} = T_{cl}$. The injected water is assumed to be in the form of vapor or the latent heat of vaporization is assumed to be taken into account in the air cooler. Based on the condition of the flow exiting the cooler ($W_{cl} = W_{sm,out}$, p_{cl}, T_{cl}, ϕ_{cl}), the dry air mass flow rate $W_{a,cl}$, the vapor mass flow rate $W_{v,cl}$, and the dry air pressure $p_{a,cl}$, can be calculated using the thermodynamic properties discussed in Section 2.3. The vapor saturation pressure is calculated from the flow temperature using Equation (2.31). Then, the vapor pressure is determined using Equation (2.30):

$$p_{v,cl} = \phi_{cl}p_{sat}(T_{cl}) \tag{2.35}$$

Because humid air is a mixture of dry air and vapor, dry air partial pressure is the difference between the total pressure and the vapor pressure:

$$p_{a,cl} = p_{cl} - p_{v,cl} \tag{2.36}$$

The humidity ratio can then be calculated from

$$\omega_{cl} = \frac{M_v}{M_a}\frac{p_{v,cl}}{p_{a,cl}} \tag{2.37}$$

where M_a is the molar mass of dry air (28.84×10^{-3} kg/mol). The mass flow rate of dry air and vapor from the cooler is

$$W_{a,cl} = \frac{1}{(1+\omega_{cl})}W_{cl} \tag{2.38}$$

$$W_{v,cl} = W_{cl} - W_{a,cl} \tag{2.39}$$

The mass flow rate of dry air remains the same for the inlet and outlet of the humidifier, $W_{a,hm} = W_{a,cl}$. The vapor flow rate increases by the amount of water injected:

$$W_{v,hm} = W_{v,cl} + W_{v,inj} \tag{2.40}$$

The vapor pressure also changes and can be calculated using Equation (2.32):

$$p_{v,hm} = \omega_{cl} \frac{M_a}{M_v} p_{a,cl} = \frac{W_{v,hm}}{W_{a,cl}} \frac{M_a}{M_v} p_{a,cl} \tag{2.41}$$

The vapor pressure $p_{v,hm}$ can then be used to determine the exit flow relative humidity

$$\phi_{hm} = \frac{p_{v,hm}}{p_{sat}(T_{hm})} = \frac{p_{v,hm}}{p_{sat}(T_{cl})} \tag{2.42}$$

Because the vapor pressure increases, the total pressure also increases:

$$p_{hm} = p_{a,cl} + p_{v,hm} \tag{2.43}$$

The humidifier exit flow rate is governed by the mass continuity

$$W_{hm} = W_{a,cl} + W_{v,hm} = W_{a,cl} + W_{v,cl} + W_{v,inj} \tag{2.44}$$

The flow leaving the humidifier enters the fuel cell cathode and thus, in the next chapter, the humidifier exit flow is referred to as cathode inlet (ca, in) flow; for example, $W_{ca,in} = W_{hm}$ and $\phi_{ca,in} = \phi_{hm}$.

The models of auxiliary components in the fuel cell system are developed in this chapter. These models will interact with the fuel cell stack model. In the next chapter, the fuel cell stack model and its submodels are described.